

## SIMULATION OF MUTUALLY DEPENDENT POLYMER FLOW AND FIBER FILLED IN POLYMER COMPOSITE DEPOSITION ADDITIVE MANUFACTURING

Z. Wang\* and D.E. Smith\*

\* Department of Mechanical Engineering, Baylor University, Waco, TX 76798

### Abstract

Short fiber-filled polymers experience increasing applications in melt extrusion additive manufacturing. As the filled polymer is melted and extruded, the fiber-filled polymer suspension exhibits mutually dependent effects, such that flow kinematics influence fiber orientation while the fiber alignment affects the formation of melt flow. This paper presents a fully-coupled numerical scheme to characterize the mutually dependent effects between melt flow and fiber orientation in a non-Newtonian axisymmetric extrusion flow including a free surface using the Galerkin Finite Element Method. The power law fluid model is employed to characterize the shear thinning rheological behaviors of polymer melts. This approach is used to solve the fully-coupled flow velocity and the fiber orientation fields for the nozzle extrusion flow in a large-scale polymer deposition additive manufacturing process. Computed results obtained from both the weakly-coupled and fully-coupled schemes exhibit notable differences in the flow velocity, fiber orientation tensor fields, die swell of free extrudate, and predicted elastic constants.

### Introduction

Polymer deposition Additive Manufacturing (AM), otherwise known as Fused Filament Fabrication (FFF), is a process where continuous thermoplastic filaments are melted and deposited on a heated bed, layer-by-layer, to build a three-dimensional (3D) object (c.f. Figure 1). The FFF technique experiences widespread application in industry for rapid prototyping of parts and tooling due to its low cost and relatively high ability to create intrinsic structures. Unfortunately, the inherent weak meso-structures of FFF-printed parts significantly reduce their stiffness and strength. Prior research shows that adding fibers to a neat polymer significantly enhanced the mechanical performance of the polymer composite structure [1-4]. The improved properties promote the applicability of FFF-created parts from design prototyping to real engineering products, especially in the promising large-scale additive manufacturing technology [5,6]. Meanwhile, adding second phase reinforcements into neat thermoplastic feedstock creates material anisotropy that significant effects the mechanical behaviors of the extruded composite [5,6]. There is still a gap in understanding how polymer composite feedstock behaves during the FFF process and the effects of processing the polymer composite on the resulting material stiffness and strength.

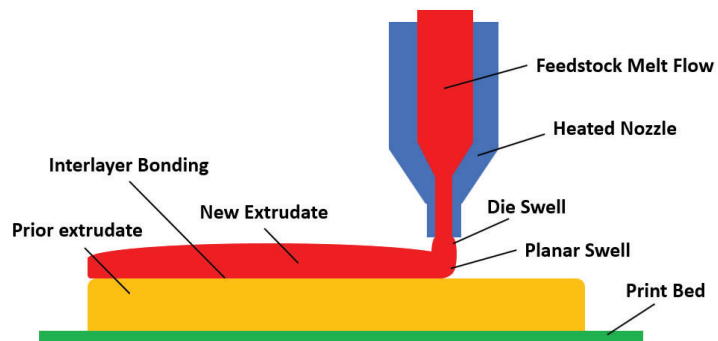


Figure 1. Featured components in a typical polymer deposition AM process.

Characterizing the behaviors of fiber reinforced polymer composite material flow is required for accurate simulation of the FFF deposition process, which has become of interest in recent years. Nixon, et al. [7] investigated fiber orientation for three FDM nozzle geometries (convergent, straight and divergent) using the commercial software Moldflow (Framingham, MA, USA). The Folgar-Tucker diffusion model [8] was implemented in the computation of fiber orientation and their results indicated that a convergent geometry nozzle yielded highest fiber alignment at the nozzle exit among those studied. While Nixon ignored the effect of die swell, Heller, et al. [9] assessed the fiber alignment in a commercial FFF printer nozzle flow with a short section of free extrudate just outside the nozzle exit. The polymer melt was modeled as a Newtonian creeping flow in the finite element program COMSOL Multiphysics (Burlington, MA, USA), and the extrudate swell was evaluated by numerically minimizing the surface normal stress integrated over the free surface. Orientation tensors based on the Advani-Tucker model [10] were employed to simulate fiber alignment. Their results showed that fiber alignment reached its peak at the boundary of the nozzle and decayed towards to the center of the extrudate. They also found that die swell reduced the longitudinal modulus of the extrudate by about 20% comparing to the material before the nozzle exit. More recently, others [9] investigated the planar swell owing to material deposition and associated fiber orientation variation [11], the Coefficient of Thermal Expansion property of the composite deposited bead [12], effects of polymer rheology modeling on the resulting predicted die swell and fiber orientation [13], and effects of swirling kinematics yielded by the single screw extrusion material feeding mechanism, on the predicted fiber orientation and associated elastic constants [14,15]. It is informative to note that given the fact that the flow fields align fiber inclusions, the fiber orientation pattern also affects the rheological properties of the suspended flow (e.g., see [10,16]). Unfortunately, most existing literature that considers flow polymer composite suspensions [7,9,11-15] are based on a weakly-coupled assumption, where the flow field is computed while neglecting the effect of fiber orientation. The weakly-coupled assumption is widely accepted for narrow gap shear-dominated flows such as those found in injection molding [17,18]. However, the fully-coupled effects between the fiber orientation and flow is noted as an important factor in identifying the process of FFF application [19], which is especially important for large-scale applications since effects of rheology-fiber coupling on a printed part will be amplified as the printing scale increases.

This study simulates the mutually dependent impacts between the polymer flow rheology and fiber reinforcement orientation in the melt extrusion process of large-scale polymer composite deposition AM through a numerical algorithm using the Galerkin Finite Element Method (GFEM) (e.g., see Reddy [20]). The polymer melt shear thinning behavior is assumed follow the generalized Newtonian fluid power law model [21]. The die swell of the free extrudate is identified through a one-dimensional remeshing technique [31]. Fiber orientation is modeled with Advani-Tucker fiber orientation tensors [10] using the orthotropic fitted closure approximation [22] and isotropic rotary diffusion [8]. This approach provides a unique insight into the process-structure-property-performance relations of the LAAM technology, thus avoiding otherwise long trial-and-error calibration processes.

### **Governing Equations**

Numerical simulation of fiber reinforced composite material flow in polymer deposition AM, including the identifications of the flow fields of the molten material, die swell, and fiber orientation state within the flow suspension, are described in this section.

### Flow Fields Kinematics

An important component of polymer extrusion AM simulations is to compute the melt flow field in the extrusion nozzle, where suspended fibers are orientated by the flow kinematics. Prior literature [9,13-15] addressed the nozzle flow characterization through a weakly-coupled formulation, where the flow field is computed as if no fibers are present in the polymer melt. As in earlier works [9,11-15], we also assume isothermal, incompressible, and highly viscous creeping flow, where the thermal gradients, inertia effect, and the time transient effect are neglected. Under these assumptions, the mass and momentum conservation equations of the flow field can be, respectively, written as [21]

$$\nabla \cdot \mathbf{v} = 0, \quad (1)$$

and,

$$\nabla \cdot \boldsymbol{\sigma} + \rho \mathbf{f} = 0, \quad (2)$$

where  $\mathbf{v}$  is the velocity vector,  $\rho$  refers to the density of the continuum,  $\mathbf{f}$  refers to the body force tensor, and  $\boldsymbol{\sigma}$  is the Cauchy stress tensor, which can be written as [21]

$$\boldsymbol{\sigma} = \boldsymbol{\tau} - P\mathbf{I}, \quad (3)$$

where  $P$  is the pressure,  $\mathbf{I}$  is the identity matrix, and  $\boldsymbol{\tau}$  is the stress tensor associated shear deformation. The latter can be written with an anisotropic contribution from fiber orientation as [22]

$$\boldsymbol{\tau} = 2\eta\mathbf{D} + 2\eta N_p \mathbb{A} : \mathbf{D}, \quad (4)$$

where  $\eta$  is the viscosity of melt, and  $N_p$  is the particle number that characterizes the intrinsic anisotropic impacts of the fibers on the flow rheology [23].  $\mathbb{A}$  is the fourth-order fiber orientation tensor which will be introduced in the following section.

### Fiber Orientation Kinetics

Characterizing the fiber orientation kinetics for filled-polymer systems in FFF additive manufacturing applications is of great importance as the final alignment of fibers in the deposited material determines the strength, stiffness and warpage of a printed part. Jeffery [24] first expressed the motion of a single rigid ellipsoidal particle in a pure shear flow. More recently, Folgar and Tucker [8] extended Jeffery's theory to analyze the interactions between fibers in a non-dilute fiber suspension by employing a fiber orientation distribution function. Further, Advani and Tucker [10] defined the fiber orientation tensor approach to quantify the fiber alignment state for concentrated suspension systems, which requires fewer independent variables than that of the Folgar-Tucker model [8]. The Advani-Tucker orientation tensor equation with isotropic rotary diffusion is written as [10]

$$\frac{D\mathbb{A}}{Dt} = (\mathbf{A} \cdot \mathbf{W} - \mathbf{W} \cdot \mathbf{A}) + \lambda(\mathbf{D} \cdot \mathbf{A} + \mathbf{A} \cdot \mathbf{D} - 2\mathbb{A} : \mathbf{D}) + 2 C_I \dot{\gamma}(\mathbf{I} - 3\mathbf{A}), \quad (5)$$

where the second- and fourth-order fiber orientation tensors are defined respectively as

$$\mathbf{A} = \langle \mathbf{p}\mathbf{p} \rangle \text{ and } \mathbb{A} = \langle \mathbf{p}\mathbf{p}\mathbf{p}\mathbf{p} \rangle, \quad (6)$$

Here,  $\mathbf{p}$  is the unit vector depicting the orientation of a single rigid fiber along the axis of fiber alignment. The angle bracket “ $\langle \rangle$ ” refers to an average over all directions, weighted by the probability distribution function of the orientation [22]. The parameter  $\lambda$  is a function of fiber geometry. For an ellipsoidal fiber,  $\lambda$  can be evaluated as [10]

$$\lambda = [(a_r)^2 - 1]/[(a_r)^2 + 1], \quad (7)$$

where  $a_r$  is the hydrodynamic aspect ratio of the ellipsoidal fiber. In Equation 5,  $C_I$  is the empirically obtained fiber interaction coefficient that provides a means for incorporating the effect of fiber-fiber interaction. Bay proposed an expression of  $C_I$  as [25]

$$C_l = 0.0184 \exp(-0.7148 v_f a_r), \quad (8)$$

where  $v_f$  refers to the fiber volume fraction of the composite system. In addition,  $\mathbf{W}$  and  $\mathbf{D}$  are the vorticity tensor and rate-of-deformation tensor of the suspension flow, respectively, which can be written as

$$\mathbf{D} = (\nabla \mathbf{v} + \nabla \mathbf{v}^T)/2 \text{ and } \mathbf{W} = (\nabla \mathbf{v} - \nabla \mathbf{v}^T)/2, \quad (9)$$

where  $\nabla \mathbf{v}$  indicates the flow gradient field and the superscript  $\mathbf{T}$  refers to the matrix transpose operation.

### Polymer Extrusion Flow Domain Model

This paper specifically focuses on the polymer composite melt flow within and just outside the extrusion nozzle of the large scale FFF process, where rheological behaviors of the filled polymer flow exhibits significant differences as compared to an unfilled event. Heller, et al. [9] (see also [13-15]) reported that the internal geometry of the nozzle has a notable impact on the fiber orientation of the extruded composite, since the flow domain geometry defined by the interior of the nozzle defines the melt flow velocity gradient fields. To eliminate the influence of the internal nozzle geometry features on our results, we do not include the turning deposition flow in this study and instead consider only the axial melt flow of the nozzle. The flow domain of interest is simplified with a 2D axisymmetric model, including the flow inside the nozzle and a short strand of free extrudate, as shown in Figure 2.

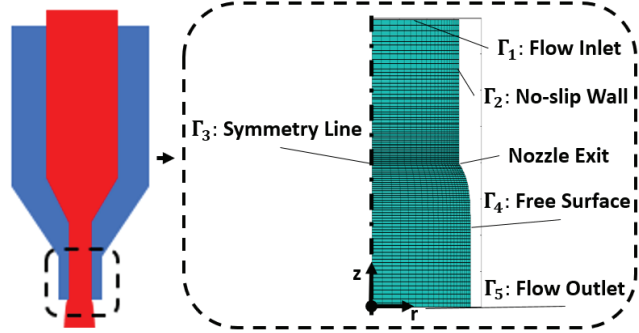


Figure 2. Boundaries of the flow domain of interest.

Based on the geometrical design of the Strangpresse large-scale additive manufacturing Model 19 single screw extruder nozzle, the radius of the straight tube that defines our flow domain is set as 0.0625 inch [13]. The ratio of the internal-nozzle length of to the radius of the nozzle is 5:1. For simplicity, the length of the free extrudate is set to be equal to the internal-nozzle length. The boundary conditions of the flow domain are labeled in Figure 2. Specifically, a fully developed velocity profile is imposed on the flow inlet. The velocity profile is computed based on the prescribed volumetric flow rate of  $1.0 \times 10^{-6} \text{ mm}^3$ , which corresponds to a mass flow rate of approximately 8 lbs/hour for 13% Carbon Fiber filled Acrylonitrile Butadiene Styrene (CF-ABS). More detail of the boundary conditions can be found in [13].

In addition, we assume an isotropic fiber orientation field for the entire flow domain as a starting point for fiber orientation calculation iterations when computing the coupled flow – fiber orientation, as in VerWeyst and Tucker [22]. Also, the hyperbolic form of Equation 5 requires an initial condition of the second-order fiber orientation tensor at the flow inlet. Herein, we imposed the fully developed fiber orientation state reported by Heller, et al. [9], assuming that the orientation state reaches a nearly steady state upstream of the flow inlet. Additionally, the fiber orientation along the no-slip boundary is prescribed as fully aligned in the flow direction [27]. The flow domain is meshed with 8-node serendipity quadrilateral elements. One of the advantages of using 8-node element is that the convergence performance of the fiber orientation equations is

much better than that obtained by using the more traditional 4-node element, even though a bit more computational cost is required. There are a total of 2000 elements with 6241 nodes in our flow model, which was found to provide a sufficient and efficient mesh quality through a mesh sensitivity study.

### **Rheology Model for Polymer Melt**

Polymer melts exhibit strong non-Newtonian flow behaviors. We herein implement the purely viscous power law fluid model to represent the shear thinning of thermoplastic composite melts. Shear thinning commonly used to model non-Newtonian behaviors of polymers such as those employed in polymer deposition additive manufacturing [21]. The viscosity of a power law fluid can be written as [21]

$$\eta(\dot{\gamma}) = K(\dot{\gamma})^{n-1}, \quad (10)$$

where  $K$  is the consistency index and  $n$  is the power-law index. In this paper, we employ the rheology properties of a 13% CF-ABS polymer at 215 °C, as reported in [14], where the power law fluid parameters are fitted as,  $K=1.2 \times 10^4$  (Pa s<sup>*n*</sup>) and  $n=0.51$ .

### **Flow-Fiber Coupling Theory**

Preceding literature [16] emphasized the importance of the mutually dependent effects between the flow suspension rheology and the fiber orientation, which serves as the basis for our fully-coupled model. Dinh and Armstrong [26] developed a rheological constitutive equation for semi-concentrated and concentrated fiber suspensions, in which the effects of fiber aspect ratio, fiber volume fraction and fiber orientation on the flow-fiber coupling intensity are provided. The Dinh-Armstrong model is commonly employed in fully coupled polymer melt flow calculations [16,27] due to its simplicity and relatively high reliability. Tucker [23] employed a dimensionless particle number  $N_p$  to characterize the intrinsic anisotropic effect of the fibers on the fiber suspensions involved with narrow gap flow applications, which appears in Equation 4. Herein, we define  $N_p$  as a function of the fiber volume fraction and fiber aspect ratio as [23,26]

$$N_p = Mv_f/(1 + Nv_f), \quad (11)$$

where  $M$  and  $N$  are coefficients related to the suspension system employed. Here,  $M$  is written as [23]

$$M = \frac{(a_r)^2}{3\ln\sqrt{\pi}/v_f} \quad (12)$$

The Dinh-Armstrong model is extended from a slender-body-theory-based model (e.g., see Batchelor [28]), which assumes that the particle's thickness can be ignored, simplifying coefficient  $N$  appearing in Equation 11 to zero. Another important feature of the slender-body assumption is that the hydrodynamic interactions between fibers can be incorporated, in an averaged sense, so that estimations beyond the dilute regime can be considered [23]. This is pivotal in the analyses the polymer composites of interest for LAAM, where most filled polymers are highly concentrated fiber suspensions. In addition, the expressions for  $N_p$  in Equations 11 and 12 assume a fully aligned fiber orientation which is supported by weakly coupled studies [9,13] simulation of fiber orientation in LAAM applications. Hence, we apply the fully alignment assumption for defining the  $N_p$ .



## Solution Approach

In this section we introduce our approaches for remeshing the free surface of the finite element domain, solving the nonlinear systems of flow and fiber orientation fields, and smoothing out the numerical instability of the nodal solutions of second-order orientation tensors.

### One-Dimensional Streamline-wise Remeshing

Identifying the location of the free surface boundary for an external flow application requires remeshing the flow domain of the free extrudate. Prior work on extrusion-based additive manufacturing modelled the melt extrusion and/or deposition process through the advanced functions provided by the finite element suite Polyflow [13-15,29,30]. Alternatively, Heller, et al. [9,11] developed a custom MATLAB (Natick, MA, USA) program to determine the optimum free surface shape by minimizing the integrated normal stress along element edges that compose the free boundary. The subroutine was in conjunction with the built-in remeshing function of COMSOL (Burlington, MA, USA). Tanner, et al. [31] computed the free surface location for an axisymmetric flow as a streamline of the flow and thus the velocity on the free boundary nodes should follow the relation

$$r_{i+1}^{(j)} = r_i^{(j)} + \int_{z_i}^{z_{i+1}} \frac{v_r}{v_z} dz, \quad (13)$$

where  $r$  is the radial direction of flow and  $z$  is the direction parallel to the flow (e.g., cylindrical coordinates appearing in Figure 2). Radii in Equation 13 are defined as shown in Figure 3 (Note, the flow domain is rotated 90 degree counterclockwise as compared to Figure 2), where the subscript  $i$  indicates successive node numbers which start at 0 with the fixed node having a radius coordinate  $r_0$  at the end of the no-slip wall. A compromise is made for the mesh around the nozzle exit to reduce the effect of stress singularity near this region [31], where moderate size elements are adopted. Otherwise, too-fine mesh results in spurious die swell profiles and too-coarse mesh yields less accurate predictions. Finally, we monitor the convergence of free surface iterations by checking the die swell ratio of the extrudate, which is written as

$$B^{(j)} = r_n^{(j)} / r_0, \quad (14)$$

where  $B$  donates the die swell ratio,  $r_n^{(j)}$  refers to the radial coordinate of the last node ( $n$ -th node) of the free surface along the flow direction at the  $j$ -th iteration. We also note that surface tension is not considered for the prediction of extrudate swell, as did in previous literature [11-15,31].

### Newton-Raphson Iteration

The GFEM formulated equations of the shear thinning flow and fiber orientation fields are both nonlinear systems, that require an appropriate numerical approach to search for the respective solutions. Prior literature employed the Newton-Raphson (N-R) iterative method in solving the proposed problems of power law fluid flow [31] and second order orientation tensor fields [22], respectively. To implement the N-R method with the GFEM formulated flow and fiber orientation problems, the tangent stiffness matrices of the systems are needed. Here, the tangent stiffness matrix of a finite-element formulate system is the derivative of the residual form of the system with respect to the primary variable (e.g., nodal velocity for the flow problem) of the system. Detail descriptions of deriving the tangent stiffness matrices for the non-Newtonian flow problem and

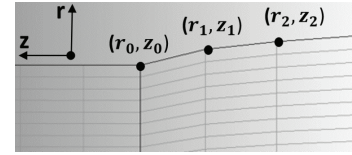


Figure 3. Schematic diagram of the streamline-wise remeshing approach.

fiber orientation problem can be found in Tanner, et al. [31] and the thesis of VerWeyst [22], separately, and will not be given here for conciseness. Additionally, the derivation of the nonlinear equations that result from employing the power-law viscosity model are beyond the scope of this paper.

### **Streamline Upwinding Petrov Galerkin Method**

The GFEM solution of the second-order fiber orientation tensor may exhibit spatial instabilities due to the lack of a diffusion term in the governing equation of Equation 5 [22]. The Streamline Upwind Petrov Galerkin (SUPG) method proposed by Brooks and Hughes [34] has been employed to spatially stabilize the solution providing a physically realistic solution alternative to the GFEM's. The SUPG method has been implemented in multiple fluid flow studies [34,35-37]. Herein, we employ an implementation proposed by Smith, et al. [37] that fits our current focus of the fiber orientation problem, where the standard GFEM arbitrary weight function is rewritten as a sum of the original weight function and an artificial diffusion term. Readers interested in the implementation of the technique are recommended to [37].

### **Program Outline**

Preceding literature [22] conducted the melt flow-fiber orientation fully coupled simulation for several internal flows by formulating Equations 1 to 5 into an integrated finite element scheme through the Galerkin Finite Element Method (GFEM) with the assistance of the commercial finite element code, FIDAP. Alternatively, we are solving the GFEM-formulated flow and fiber orientation problem, including die swell, with a customized MATLAB code. Integrated nonlinear problems, such as the flow-fiber coupling, seldom converge even with the delicate numerical treatments introduced above. Therefore, we decompose the system into two sub parts: the flow module, which numerically solves Equations 1 to 4, and 10, and the fiber orientation module, which numerically evaluates Equation 3. The algorithm starts by computing the polymer melt flow field assuming a known fiber orientation field. Then the extrudate swell ratio of the computed free surface location is evaluated through Equation 13. With the computed flow kinematics, nodal fiber orientation tensors are computed with a time-marching forward Euler method [38]. The time-marching scheme stops once a steady state of the fiber orientation reaches (e.g., difference between two successive solutions are trivial). It is important to note that the time step for the fiber orientation problem is sensitive to the dimensions of the flow domain. Herein, we employ a fixed step of 0.01, which yields an efficient convergent trial. After the computation of the fiber orientation module, the flow fields are updated with the solved fiber orientation results. The iteration between the two sub-modules keeps running until a convergence is achieved ultimately.

### **Results and Discussion**

A two-dimensional axisymmetric flow model simulating the polymer composite melt extrusion of a LAAM system is considered using the developed code. Computed results of the weakly-coupled and fully-coupled systems of the flow fields appear first. The extruder die swell profiles of the vertical extrudate are given. Comparison between the fiber orientation tensor fields solved in the weakly-coupled and fully-coupled schemes is presented. In addition, we employ the orientation homogenization [10] method to estimate the effective elastic constants of an extruded 13% CF-ABS polymer composite, where two different fiber aspect ratios are considered.

### ***Flow Kinematics within the Polymer Melt Flow***

The flow kinematics within the nozzle and just outside the nozzle exit is of great importance as this flow field orientates the fiber suspension in the final product, and thus determine the mechanical performances of the solidified printed structure. The weakly-coupled and fully-coupled solution of velocity field appear in Figure 4, where both  $v_r$  and  $v_z$  are shown. We define the velocity field along the flow direction as  $v_z$ , and that perpendicular to the direction of flow is referred as  $v_r$  (c.f. Figure 2 for the definition of 2D cylindrical r-z coordinates). For fully-coupled simulation, the fiber aspect ratio and fiber volume fraction are 15 (same values as in [9,11]) and 0.13 (which corresponds to the applied 13% CF-ABS material model), respectively.

Velocity contours indicate that the flow field of  $v_z$  is one or more orders of magnitude higher than that of  $v_r$  in most area of the flow domain, except near the nozzle exit. Variations in the velocity fields at the nozzle exit are due to the change in the flow boundary condition, where the melt flow is leaving the region having a constrained no-slip wall and entering a region where the boundary is free of this limitation. As seen in figure 4, the velocity component  $v_r$  increases by nearly an order of magnitude near the outer intersection of boundaries of no-slip wall and free surface. In contrast, changes in  $v_z$  occurs along the radial direction across the nozzle exit, such that  $v_z$  near the free surface boundary increases while the velocity near the center of the nozzle decreases, as expected. Values of  $v_z$  become uniform across the radial direction as flow progresses towards the flow domain exit. As a result, a contraction flow occurs along the centerline of the nozzle which is known to have a significant effect on fiber orientation [9,13]. In addition, it can be seen that contours of  $v_r$  and  $v_z$  in the fully-coupled solution exhibits a notable variation as compared to the weakly-coupled case.

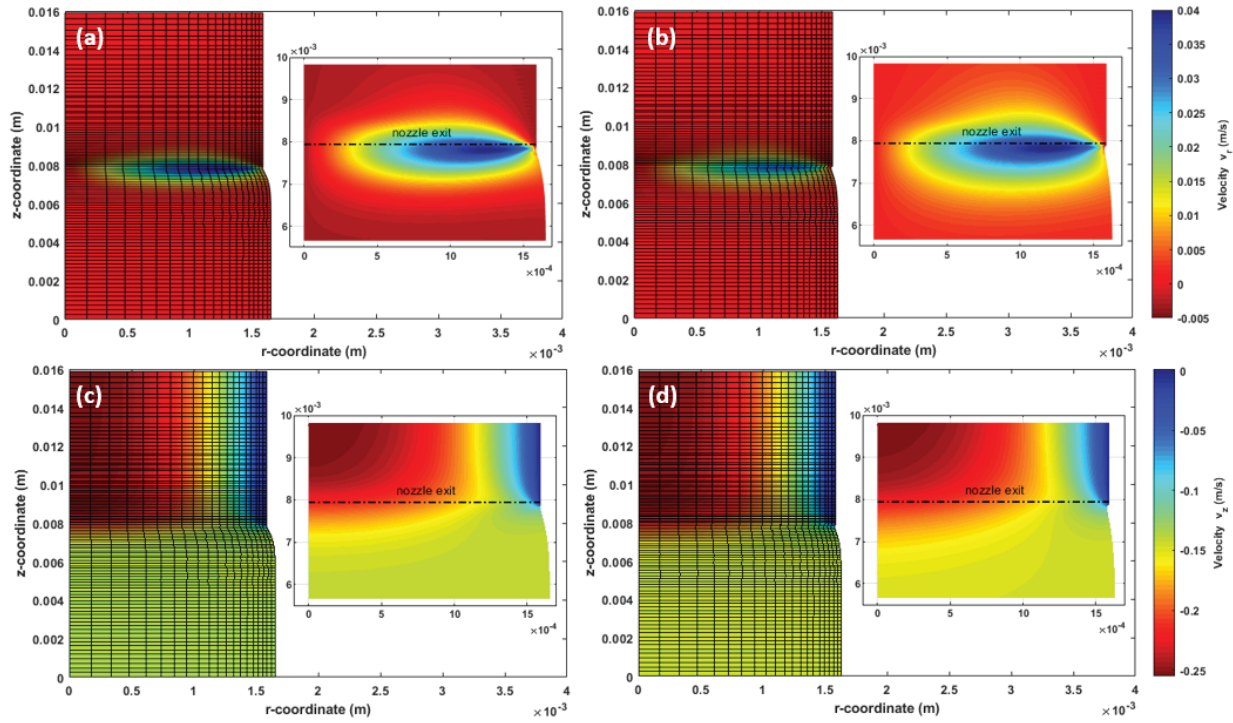


Figure 4. Computed contours of flow fields: (a) weakly-coupled velocity  $v_r$ ; (b) fully-coupled velocity  $v_r$ ; (c) weakly-coupled velocity  $v_z$ ; (d) fully-coupled velocity  $v_z$ .



From the flow contours appearing in Figure 4, it is seen that the die swell of the free extrudate varies significantly between the weakly-coupled and fully-coupled solutions, which can be clearly observed through Figure 5. A significant reduction is seen between the weakly-coupled and fully-coupled die swell profiles of the free extrudate. Specifically, it is also seen that there is a distortion toward the axis of symmetry at the beginning of free extrudate, which is also observed in our previous work (c.f. Figure 8 in reference [13]). Die swell results appearing in Figure 5 show that the presence of fibers has a significant effect on the stress field within the melt flow, especially the normal stress field that directly contributes to the die swell. Future work of this study should also include the characterization of the stress fields of the melt flow assuming other rheology models including the viscoelastic fluid models.

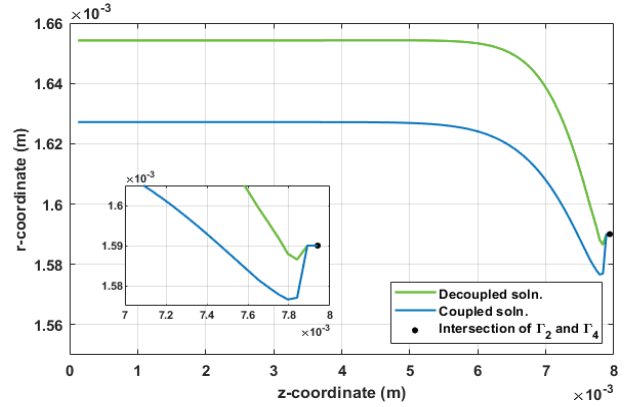


Figure 5. Predicted free surface of the extrudate solved by weakly-coupled and fully-coupled schemes. Note, the radius of the fixed nozzle is 1.59 mm.

### ***Fiber Orientation Kinetics of the Domain***

It is important to notice that while the flow domain is created in cylindrical coordinates as defined in Figure 2, the fiber orientation tensor fields are solved in three-dimensional (3D) Cartesian coordinates, where the velocity gradients computed in cylindrical coordinates are transformed into Cartesian coordinates (e.g., see Heller [9]) prior to computing orientation tensor components. It follows that the 1,2,3 subscripts of the second-order orientation tensor correspond to the  $r, \theta, z$ , separately for 3D cylindrical coordinate space. Computed values of  $A_{33}$  are given in Figure 6, which indicates how well the fibers are aligned along the principal flow direction. In addition, the principal direction of  $\mathbf{A}$  appears as a field of directed line segments superimposed over the  $A_{33}$  field near the nozzle exit, where the fiber orientation state experiences a significant change. Note, the magnitude and direction of each line segment is determined by the largest eigenvalue of the nodal solution of  $\mathbf{A}$  and its associated eigenvector, respectively [22].

Computed results show that the fiber alignment in the flow direction within the nozzle is small, while the flow near the no-slip wall exhibits slightly higher principal flow-direction alignment due to high shear stress near the boundary. Once the flow leaves the constrained nozzle, the orientation state is more characterized by a principal fiber alignment which increases gradually from the center of the flow to the free surface boundary. In addition, it is clearly seen that the fully-coupled solution results in a higher principal fiber alignment than the weakly-coupled solution over the entire domain. Recall, the magnitude of the fully-coupled flow field along extrusion direction also increases as compared to the weakly-coupled solution, as shown in Figure 4. High shear within the flow domain is enhanced by the induced fiber alignment, which promotes the same fiber alignment along the flow direction. Prior experimental works reported that the shear rate of fill-polymer melt exhibits a higher order of magnitude as compared to the unfilled polymer system in rheology tests of melt extrusion [39,40], supporting our numerical results.

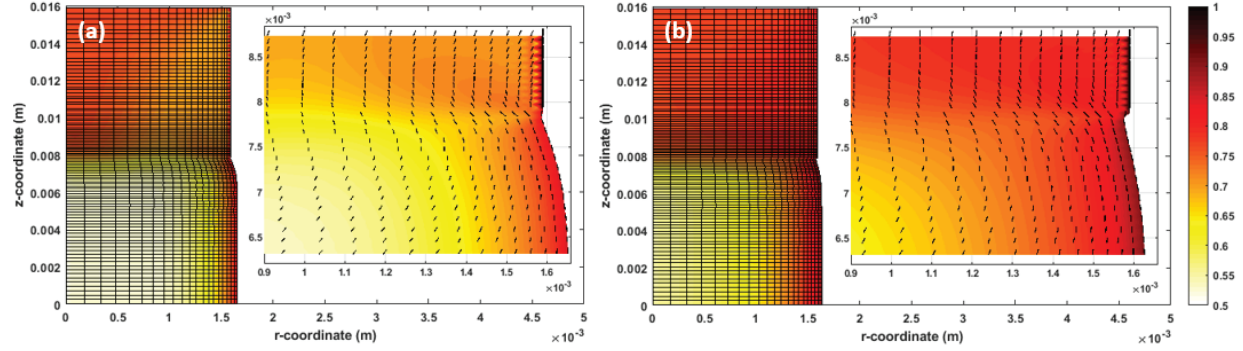


Figure 6. Computed contours (and vector plots of  $\mathbf{A}$ ) of second order orientation tensor  $A_{33}$ : (a) weakly-coupled solution; (b) fully-coupled solution.

Once fiber orientation tensors are computed throughout the flow domain, an estimate of the elastic properties of a polymer composite extrudate may be obtained which provides information for evaluating the mechanical performance of a LAAM-printed part. Here, we assume the fiber orientation tensor at the flow exit reaches a steady state that represents fiber alignment within an extrudate that is about to be deposited onto a substrate. The local stiffness matrix,  $\tilde{\mathbf{C}}_{ijkl}$ , of an extruded composite material can be computed using  $\mathbf{A}$  and  $\mathbf{\bar{A}}$  by employing the orientation homogenization method (e.g., see [10]) which combines a micromechanical model (e.g., Tandon-Weng method as in [13]). The effective bead stiffness tensor  $\bar{\mathbf{C}}_{ijkl}$  of the overall composite material is evaluated as the integrated average over the cross-section of the extrudate as

$$\bar{\mathbf{C}}_{ijkl} = \frac{1}{\pi r_B^2} \int_0^{2\pi} \int_0^{r_B} (\tilde{\mathbf{C}}_{ijkl} \cdot \mathbf{r}) dr d\theta, \quad (15)$$

which we evaluate numerically using the trapezoidal rule as in [38]. In the above,  $r_B$  is the radius of the free extrudate at the flow domain exit. Evaluating elastic constants from the stiffness tensor  $\bar{\mathbf{C}}_{ijkl}$  is performed in the usual manner (c.f. [41]) which is omitted here for conciseness. We utilize the 13% CF-ABS as the material model, as mentioned above. The elastic constants of the constituent phases are given in Table 1, where  $E$ , and  $\nu$  indicate the Young's modulus (or axial modulus) and Poisson's ratio, respectively.

Table 1. Elastic constants of the constituents of a 13% CF-ABS [13].

Material	$E$ (GPa)	$\nu$
ABS matrix	2.25	0.35
Carbon fiber	230	0.2

The predicted elastic constants along three coordinate directions appear in Table 2, where two fiber aspect ratio values are considered since this parameter is an important contributor to elastic property prediction. From the computed results it is shown that the values of the predicted moduli  $\bar{E}_{11}$  to  $\bar{E}_{33}$  increase with increased fiber aspect ratio. In addition, the weakly-coupled and fully-coupled solutions also exhibit notable difference, where  $\bar{E}_{11}$  to  $\bar{E}_{33}$  obtained from the fully-coupled scheme are higher than those from the weakly-coupled solution. Particularly, the highest variation among the predicted properties is seen on  $\bar{E}_{33}$  which is the modulus along the flow direction, where most fibers align as shown in Figure 6. Here, the Partial Relative Difference (PRD) (c.f. Equation 13 in reference [12]) is adapted to quantify the differences of data appear in Table 2. In detail,  $\bar{E}_{33}$  values computed in the weakly-coupled and the fully-coupled simulations

vary by 15.8% for a 13% CF-ABS at  $a_r=15$ . Additionally, the PRD of  $\bar{E}_{33}$  between the fully-coupled and weakly-coupled cases with  $a_r=10$  and  $a_r=15$  is even higher at 29.6%. Computed results herein shown that the flow-fiber coupling effects can be extremely important in understanding the process-structure-property-performance relations in melt extrusion process of a LAAM application.

Table 2. Effective elastic constants predicted with different parameters applied.

$a_r$	A solution	$\bar{E}_{11}$ (GPa)	$\bar{E}_{22}$ (GPa)	$\bar{E}_{33}$ (GPa)
10	weakly-coupled	3.22	3.60	4.95
10	fully-coupled	3.18	3.53	5.33
15	weakly-coupled	3.41	4.02	6.13
15	fully-coupled	3.29	3.80	7.18

### Summary

A finite-element-based algorithm is developed for numerical characterization of the melt flow-fiber orientation coupling effects on polymer composite melt flow in polymer deposition Large Area Additive Manufacturing (LAAM). The governing equations of the flow and fiber orientation problems are formulated by the Galerkin Finite Element Method. The generalized Newtonian fluid power law model is employed to model the shear thinning viscosity of polymer melts. The Streamline-Upwind Petrov Galerkin method is used to address the numerical instability. A one-dimensional spine remeshing technique is applied to identify the location of free extrudate die swell surface. Developed code is employed in solved the coupled flow-fiber orientation solutions of an axial extrusion flow with a free surface.

Computed results indicate that orientation tensor component values for fully-coupled solutions yield higher alignment along the extrusion direction as compared to those from the weakly-coupled solution. In addition, the predicted die swell ratio reduces when the fully-coupled fiber orientation is included in the flow computation. The coupling scheme between melt flow and fiber orientation fields also play a pivotal role in determining the elastic properties of a polymer composite extrudate, where the PRD between the weakly-coupled and the fully-coupled computed  $\bar{E}_{33}$  component is 16%. In addition, increasing the fiber aspect ratio also increases the elastic constants notably, where the highest PRD is seen to be as high as 30%.

### Acknowledgements

The authors would like to acknowledge the financial support from Department of Mechanical Engineering at Baylor University. We would also like to acknowledge the Strangpresse Corporation for donating the Model-19 large-scale additive manufacturing single screw extruder that facilitates us to build up a LAAM system for learning the material deposition process. We also greatly appreciate many beneficial fiber orientation discussions with Dr. David Jack at Baylor University.

## References

- [1] R.W. Gray, D.G. Baird, and J.H. Bohn. Effects of processing conditions on short TLCP fiber reinforced FDM parts. *Rapid Prototyping Journal*, 4(1):14–25, 1998.
- [2] R.W. Gray, D.G. Baird, and J.H. Bohn. Thermoplastic composites reinforced with long fiber thermotropic liquid crystalline polymers for fused deposition modeling. *Polymer Composites*, 19(4):383–394, 1998.
- [3] W. Zhong, F. Li, Z. Zhang, L. Song, and Z. Li. Short fiber reinforced composites for fused deposition modeling. *Materials Science and Engineering*, A301:125–130, 2001.
- [4] S.H. Masood and W.Q. Song. Development of new metal/polymer materials for rapid tooling using fused deposition modelling. *Materials and Design*, 25:587–594, 2004.
- [5] Love, L. J., et al. "The importance of carbon fiber to polymer additive manufacturing." *Journal of Materials Research* 29.17 (2014): 1893-1898.
- [6] Duty, C. E., et al. "Structure and mechanical behavior of Big Area Additive Manufacturing (BAAM) materials." *Rapid Prototyping Journal* 23.1 (2017): 181-189.
- [7] Nixon, J., et al. "Three parameter analysis of fiber orientation in fused deposition modeling geometries." *Proc. of PPS conference*. 2014.
- [8] Folgar, F., and C. L. Tucker III. "Orientation behavior of fibers in concentrated suspensions." *Journal of reinforced plastics and composites* 3.2 (1984): 98-119.
- [9] Heller, B., Smith, D.E., Jack, D.A., The Effects of Extrudate Swell, Nozzle Shape, and the Nozzle Convergence Zone on Fiber Orientation in Fused Deposition Modeling Nozzle Flow. In *American Society of Composites-30th Technical Conference* 2015 Nov 2.
- [10] Advani S.G., Tucker, C.L., The use of tensors to describe and predict fiber orientation in short fiber composites. *Journal of rheology*. 1987 Nov;31(8):751-84.
- [11] Heller, B., Smith, D.E., Jack, D.A. "Planar deposition flow modeling of fiber filled composites in large area additive manufacturing." *Additive Manufacturing* 25 (2019): 227-238.
- [12] T. Russell, B. Heller, D. A. Jack, and D. E. Smith, "Prediction of the Fiber Orientation State and the Resulting Structural and Thermal Properties of Fiber Reinforced Additive Manufactured Composites Fabricated Using the Big Area Additive Manufacturing Process," *J. Compos. Sci.*, vol. 2, no. 2, p. 26, 2018.
- [13] Z. Wang and D. E. Smith, "Rheology Effects on Predicted Fiber Orientation and Elastic Properties in Large Scale Polymer Composite Additive Manufacturing," *J. Compos. Sci.*, vol. 2, no. 1, p. 10, 2018.
- [14] Z. Wang, and D. E. Smith. "Screw Swirling Effects on Fiber Orientation Distribution in Large-Scale Polymer Composite Additive Manufacturing." *Proceedings of the Solid Freeform Fabrication Symposium*, Austin, TX, USA. 2018.
- [15] Wang, Zhaogui, and Douglas E. Smith. "Numerical analysis of screw swirling effects on fiber orientation in large area additive manufacturing polymer composite deposition." *Composites Part B: Engineering* (2019): DOI: 10.1016/j.compositesb.2019.107284.
- [16] Lipscomb, G. G.; Denn, M. M.; Hur, D. U.; Boger, D. V. The flow of fiber suspensions in complex geometries. *J. Non-Newton. Fluid Mech.* 1988, 26, 297–325.
- [17] Bay, Randy S., and Charles L. Tucker III. "Fiber orientation in simple injection moldings. Part I: Theory and numerical methods." *Polymer composites* 13.4 (1992): 317-331.
- [18] Advani, Suresh G., and Charles L. Tucker III. "A numerical simulation of short fiber orientation in compression molding." *Polymer composites* 11.3 (1990): 164-173.
- [19] Brenken, Bastian, et al. "Fused filament fabrication of fiber-reinforced polymers: A review." *Additive Manufacturing* 21 (2018): 1-16.
- [20] Reddy, J. N. (1993). *An introduction to the finite element method*. New York.
- [21] Baird, Donald G., and Dimitris I. Collias. *Polymer processing: principles and design*. John Wiley & Sons, 2014.
- [22] VerWeyst, Brent E., and Charles L. Tucker III. "Fiber suspensions in complex geometries: Flow/orientation coupling." *The Canadian Journal of Chemical Engineering* 80.6 (2002): 1093-1106.

- [23] Tucker, C. L. Flow regimes for fiber suspensions in narrow gaps. *J. Non-Newton. Fluid Mech.* 1991, 39, 239–268.
- [24] Jeffery, George Barker. "The motion of ellipsoidal particles immersed in a viscous fluid." *Proceedings of the Royal Society of London. Series A, Containing papers of a mathematical and physical character* 102.715 (1922): 161-179.
- [25] R.S. Bay, *Fiber Orientation in Injection Molded Composites: A Comparison of Theory and Experiment*, Ph.D. Thesis University of Illinois Urbana-Champaign, 1991.
- [26] Dinh, Steven M., and Robert C. Armstrong. "A rheological equation of state for semiconcentrated fiber suspensions." *Journal of Rheology* 28.3 (1984): 207-227.
- [27] Ranganathan, Sridhar, and Suresh G. Advani. "A Coupled Solution for the Fiber Orientation and Rheology of Non-Dilute Short Fiber Suspensions in Radial Flow." *Theoretical and Applied Rheology*. Elsevier, 1992. 874-876.
- [28] Batchelor, G. K. (1971). The stress generated in a non-dilute suspension of elongated particles by pure straining motion. *Journal of Fluid Mechanics*, 46(4), 813-829.
- [29] Bellini, William J., and Rita F. Helfand. "The challenges and strategies for laboratory diagnosis of measles in an international setting." *Journal of infectious diseases* 187.Supplement 1 (2003): S283-S290.
- [30] Watanabe, Narumi. *Computational and experimental investigation of reinforced polymers for material extrusion additive manufacturing*. Diss. Georgia Institute of Technology, 2016.
- [31] Tanner, R. I., Nickell, R. E., & Bilger, R. W. (1975). Finite element methods for the solution of some incompressible non-Newtonian fluid mechanics problems with free surfaces. *Computer Methods in Applied Mechanics and Engineering*, 6(2), 155-174.
- [32] Householder, A. S. (2006). *Principles of numerical analysis*. Courier Corporation.
- [33] Ben-Israel, A. (1966). A Newton-Raphson method for the solution of systems of equations. *Journal of Mathematical analysis and applications*, 15(2), 243-252.
- [34] Brooks, Alexander N., and Thomas JR Hughes. "Streamline upwind/Petrov-Galerkin formulations for convection dominated flows with particular emphasis on the incompressible Navier-Stokes equations." *Computer methods in applied mechanics and engineering* 32.1-3 (1982): 199-259.
- [35] Swaminathan, C. R., & Voller, V. R. (1992). Streamline upwind scheme for control-volume finite elements, part I. Formulations. *Numerical Heat Transfer, Part B Fundamentals*, 22(1), 95-107.
- [36] Yu, C. C., & Heinrich, J. C. (1987). Petrov—Galerkin method for multidimensional, time-dependent, convective-diffusion equations. *International Journal for numerical methods in engineering*, 24(11), 2201-2215.
- [37] Smith, Douglas E., Daniel A. Tortorelli, and Charles L. Tucker III. "Optimal design for polymer extrusion. Part II: Sensitivity analysis for weakly-coupled nonlinear steady-state systems." *Computer Methods in Applied Mechanics and Engineering* 167.3-4 (1998): 303-323.
- [38] Chapra, S. C., & Canale, R. P. (1998). *Numerical methods for engineers (Vol. 2)*. New York: Mcgraw-hill.
- [39] Jain, Sachin, et al. "Strong decrease in viscosity of nanoparticle-filled polymer melts through selective adsorption." *Soft Matter* 4.9 (2008): 1848-1854.
- [40] Hideyuk, et al. "Origin of Reduction in Extrudate Swell of Molten Polymer by Adding of Rigid Fillers." *Journal of Textile Engineering* 64.4 (2018)..
- [41] Gould, P. L., & Feng, Y. (1994). *Introduction to linear elasticity*. New York: Springer-Verlag.